Available online at www.sciencedirect.com
SCIENCE DIRECT®
Journal of Sound and Vibration 262 (2003) 391–417
JOURNAL OF SOUND AND VIBRATION
www.elsevier.com/locate/jsvi

Flexible polyurethane foam modelling and identification of viscoelastic parameters for automotive seating applications

R. Deng, P. Davies*, A.K. Bajaj

Ray W. Herrick Laboratories, School of Mechanical Engineering, Purdue University, West Lafayette, IN 47907-1077, USA

Received 28 January 2002; accepted 23 October 2002

Abstract

A hereditary model and a fractional derivative model for the dynamic properties of flexible polyurethane foams used in automotive seat cushions are presented. Non-linear elastic and linear viscoelastic properties are incorporated into these two models. A polynomial function of compression is used to represent the non-linear elastic behavior. The viscoelastic property is modelled by a hereditary integral with a relaxation kernel consisting of two exponential terms in the hereditary model and by a fractional derivative term in the fractional derivative model. The foam is used as the only viscoelastic component in a foam–mass system undergoing uniaxial compression. One-term harmonic balance solutions are developed to approximate the steady state response of the foam–mass system to the harmonic base excitation. System identification procedures based on the direct non-linear optimization and a sub-optimal method are formulated to estimate the material parameters. The effects of the choice of the cost function, frequency resolution of data and imperfections in experiments are discussed. The system identification procedures are also applied to experimental data from a foam–mass system. The performances of the two models for data at different compression and input excitation levels are compared, and modifications to the structure of the fractional derivative model are briefly explored. The role of the viscous damping term in both types of model is discussed.

1. Introduction

Flexible polyurethane foams are widely used in engineering applications, especially in automotive seat cushions because they can provide degrees of comfort and protection not achieved by any other single material. Since many seats are all-foam, by tuning the foam properties it is possible to control the quasi-static and dynamic comfort of the seat occupant.

*Corresponding author. Tel.: +1-765-494-9274; fax: +1-765-494-0787.
E-mail address: daviesp@ecn.purdue.edu (P. Davies).

0022-460X/03/$ - see front matter
doi:10.1016/S0022-460X(03)00104-4

However, much of the seat design in the automotive industry is based on experience from previous designs without the benefit of a clear understanding of the properties of the foams used in the seat cushions. Seat designers need seat-occupant models that incorporate accurate models of foam behavior. Therefore, there is a strong need to characterize the quasi-static and dynamic properties of foam.

As reported in Refs. [1,2], the quasi-static behavior of foam is significantly different from its dynamic behavior. The dynamic properties also depend on the compression level and the excitation amplitude [3,4]. Even at low excitation levels, foam can exhibit non-linear behavior [5]. Based upon a combination of observation and modelling of the foam material and the fluid contained in the foam, models have been proposed that incorporate non-linear elastic elements [5] and non-linear damping elements [7]. Because of the viscoelastic behavior [8,9], foam does not recover immediately after the loading is released, i.e., the previous loading history affects the current status. Depending on the type of foam, it may take several days to recover completely. Creep and relaxation behavior are two manifestations of the viscoelastic properties of foam [10,11].

Several types of models are used to characterize the uni-directional linear viscoelastic behavior of foam. Sometimes, arrangements of springs and dashpots (Kelvin and Maxwell elements) are used [10,12]. Other researchers [5,13,14] have modelled the relationship between stress and strain in the foam as [15]

$$\sigma(t) = E\left(\epsilon(t) - \int_0^t \Gamma(t-\tau)\epsilon(\tau)\,\mathrm{d}\tau\right), \tag{1}$$

where $\Gamma(t-\tau)$ is the material's relaxation kernel, E is the instantaneous modulus, $\sigma(t)$ is the stress, and $\epsilon(t)$ is the strain. This is commonly referred to as the 'hereditary model'. The relaxation kernel $\Gamma(t-\tau)$ is often taken to be the summation of exponential terms [13]:

$$\Gamma(t-\tau) = \sum_{i=1}^{N} a_i \mathrm{e}^{-\alpha_i(t-\tau)}, \tag{2}$$

where the viscoelastic parameters a_i and α_i, $i = 1, 2, \ldots N$, are either real constants or occur in complex conjugate pairs.

Fractional derivative models have also been used to describe behavior of viscoelastic materials such as foam and rubber [16–18]. Bagley and Torvik [19] provided the theoretical basis for the use of fractional derivative models to characterize viscoelasticity. In these models, the differential constitutive relation is generalized by including derivatives with a fractional order [30] and the stress–strain relationship takes the form

$$\sigma(t) + E_s D^{\alpha_1}\sigma(t) = E_0\epsilon(t) + E D^{\alpha_2}\epsilon(t), \tag{3}$$

where D^{α_i} is the fractional derivative operator defined below in Eq. (8) and the fractional orders α_i are usually between 0 and 1.

Two models of the uni-directional motion of the foam–mass system shown in Fig. 1 are considered here. Both models include non-linear elastic elements in the form of an odd-order polynomial. To model the viscoelastic behavior one model incorporates the hereditary description in Eq. (1) and the other model incorporates the fractional derivative description of Eq. (3). System

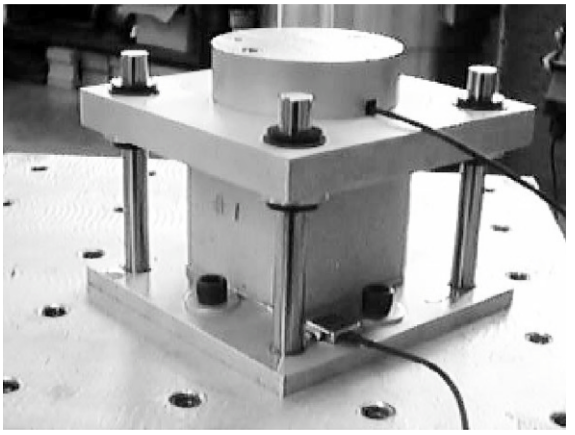

Fig. 1. The experimental rig for dynamic testing of foam–mass system.

identification techniques are then developed based on approximate one-term harmonic balance solutions of the resulting equations for the one degree-of-freedom dynamic system. These techniques are applied to simulation as well as experimental data, and results of their effectiveness are reported. We should note that both White et al. [3] and Singh et al. [6] studied the same physical system and used the 'hereditary model' to characterize the viscoelastic properties of foam. While White et al. [3] used a model with $N = 1$ for the relaxation kernel, the latter authors showed that a model with $N = 2$ and complex conjugate terms gives much better results. In the present work, the hereditary model used is again with $N = 2$ though the identification problem is reformulated in a more direct way.

This paper is organized as follows: the non-linear viscoelastic models for uni-directional response of the foam–mass system are first described in Section 2. This is followed by a discussion of frequency responses corresponding to the two linear models. Then, the harmonic response approximation for the complete non-linear model is developed using the method of harmonic balance. These equations are then used in a system identification procedure in Section 3 to estimate the non-linear elastic and linear viscoelastic model parameters for the two types of models. Sensitivity of the identification procedure to the choice of cost function, resolution of data and presence of noise is investigated. Finally, in Section 4, the procedure is applied to experimental data and results of the estimated parameters for the two models are compared. The conclusions of the work are summarized in Section 5.

2. Non-linear and viscoelastic models of foam

The two models of the dynamic, uni-directional behavior of the foam–rigid block (mass) system shown in Fig. 1 are

$$m\ddot{x} + c\dot{x} + kx + k_3x^3 + k_5x^5 - k\int_{-\infty}^{t} \sum_{i=1}^{N} a_i e^{-\alpha_i(t-\tau)}x(\tau)\,d\tau = f(t) \tag{4}$$

and

$$m\ddot{x} + c\dot{x} + kx + k_3x^3 + k_5x^5 + aD^{\alpha}x = f(t). \tag{5}$$

These will be referred to in the rest of the paper as the hereditary model and the fractional derivative model, respectively. m is the mass of the rigid block, k_3 and k_5 are the third- and fifth order stiffness coefficients, c is a viscous damping coefficient, and $f(t)$ is the external force. In the hereditary model N was chosen to be 2, which has been found to give better results than an $N = 1$ model, but still may be lower than the optimal value [5]. The exponents (α_1 and α_2) were taken to be complex conjugate pairs because in previous research [6] models with complex conjugate values were found to give better response predictions than models with real viscoelastic parameters. In the simplified version of the fractional derivative model the fractional derivative order (α) and the coefficient of this term (a) are the viscoelastic parameters. The term in Eq. (3) corresponding to the derivative of the instantaneous stress is assumed to be zero.

2.1. Linear hereditary model behavior

This model was studied in detail by Singh [5] and only a brief discussion is given here of the influence of the viscoelastic terms on the linear model behavior. The frequency response of the linear hereditary model is

$$H(\mathrm{j}\omega) = \frac{X(\mathrm{j}\omega)}{F(\mathrm{j}\omega)} = \frac{1}{-m\omega^2 + \mathrm{j}c\omega + k - kP(\mathrm{j}\omega)}, \tag{6}$$

where $P(\mathrm{j}\omega) = \sum_{i=1}^{N} a_i/(\mathrm{j}\omega + \alpha_i)$, and for $N = 2$, $P(\mathrm{j}\omega) = (2\mathrm{j}a_r\omega + 2(\alpha_r a_r + \alpha_i a_i))/(-\omega^2 + \mathrm{j}2\alpha_r\omega + |\alpha|^2)$.

Based on earlier experimental results [5], model parameter values were chosen to be: $N = 2$, $m = 1$ kg, $c = 10$ N s/m, $k = 2500$ N/m, $a_{1,2} = -0.44 \pm 4.98\mathrm{i}\ \mathrm{s}^{-1}$, $\alpha_{1,2} = 29.23 \pm 6.57\mathrm{i}\ \mathrm{s}^{-1}$. To visualize the influence of the viscoelastic terms on the frequency response magnitude, $\angle a_1$ was varied from 0° to 180° and $|a_i|$ was varied form 0.1 to 30. The results are shown in Figs. 2(a) and (b), respectively. Results of varying $\Im(\alpha_1)$ from 0 to 90 are shown in Fig. 2(c), and results of varying $\Re(\alpha_1)$ from 5 to 120 are shown in Fig. 2(d).

As shown in Fig. 2(a), for a fixed value of $|a_1|$, the peak of $|H(\mathrm{j}\omega)|$ becomes more dominant and shifts to higher frequencies as the phase of the coefficient a_1 increases. This effect is very similar to decreasing viscous damping (c) in a mass–spring–damper system. For the case where the magnitude of the coefficient $|a_1|$ is increased while keeping the phase ($\angle a_1$) constant, the peak amplitude of the frequency response decreases, while the resonance frequency increases (see Fig. 2(b)). Therefore, an increase in $|a_1|$ appears to lead to an increase in both the equivalent stiffness and the equivalent damping in the overall system.

The variation of the frequency response as a function of parameter α_i is more complicated, as shown in Figs. 2(c) and (d). When the imaginary part of α_1 increases and its real part is fixed, the peak amplitude in the spectrum first decreases and shifts slightly to the right, indicating an increase in damping and stiffness. As $\Im(\alpha_1)$ is increased beyond a critical value, the resonance frequency starts to decrease and the peak amplitude decreases as well. This is followed by an increase in peak magnitude and resonance frequency as $\Im(\alpha_1)$ is further increased. As shown in

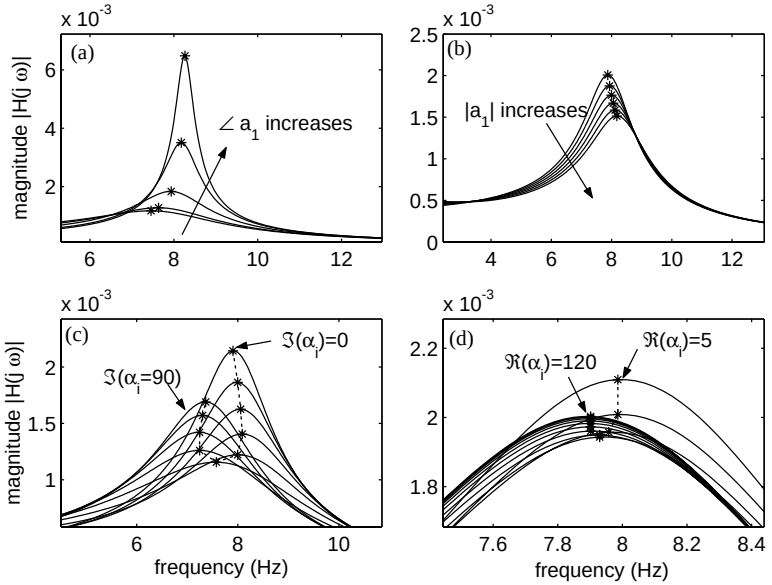

Fig. 2. The effect of variations in a_i and α_i on the frequency response of the linear hereditary model. $m = 1$ kg, $c = 10$ N s/m, and $k = 2500$ N/m. (a) $|a_i| = 5, \arg(a_1)$: 0–180°, $\alpha_{1/2} = 29.23 \pm 6.57$i, (b) $\arg(a_1) = 92°$, $|a_i|$: 0.1–30, $\alpha_{1,2} = 29.23 \pm 6.57$i, (c) $\Re(\alpha_i) = 29.23$, $\Im(\alpha_1)$: 0–90 rad/s, $a_{1,2} = -0.44 \pm 4.98$i, (d) $\Im(\alpha_1) = 6.75$ rad/s, $\Re(\alpha_i)$: 5–120, $a_{1,2} = -0.44 \pm 4.98$i.

Fig. 2(d), when the real part of α_1 is varied between 5 and 120 and the imaginary part is fixed, the damping appears first to increase and then decrease, while the frequency at which the peak occurs also gets smaller as the real part of α_1 increases. The changes in resonance frequency then are quite small, thus indicating that $\Re(\alpha_1)$ only has a small influence on the equivalent stiffness of the system.

The above results illustrate that the viscoelastic terms can influence the overall stiffness and viscous damping of the system, but the relationship is quite complex and the trends here may not be universal. Changes in the values of the other fixed parameters may lead to different types of changes as a particular viscoelastic parameter is varied. It is clear that the behavior is much more complicated than that for a classical spring–damper model, and this may be advantageous when modelling the complex properties of foam materials.

2.2. Characteristics of the linear fractional derivative model

The fractional operator is a generalization of the ordinary differential operator to the order of fractional values. The most widely used definition of an integral of fractional order is via a transformation called the Riemann–Liouville integral [20]:

$$D^{\alpha}\{x(t)\} = \frac{\mathrm{d}^{\alpha}x(t)}{\mathrm{d}t^{\alpha}} = \frac{1}{\Gamma(-\alpha)}\int_0^t \frac{x(\tau)}{(t-\tau)^{\alpha+1}}\,\mathrm{d}\tau, \quad \alpha < 0, \tag{7}$$

where $\Gamma(x)$ is the gamma function. For $\alpha > 0$, the case considered here, one can utilize

$$D^{\alpha}\{x(t)\} = \frac{\mathrm{d}^{\alpha}x(t)}{\mathrm{d}t^{\alpha}} = \frac{\mathrm{d}^{n}}{\mathrm{d}t^{n}}\left[\frac{1}{\Gamma(n-\alpha)}\int_{0}^{t}\frac{x(\tau)}{(t-\tau)^{\alpha-n+1}}\,\mathrm{d}\tau\right], \tag{8}$$

in which n is the smallest integer that is larger than α. With this definition of the convolution integral, the fractional derivative model readily demonstrates the dependence of the current state on the history of response. Also, it is a fading memory operator in that it weights the recent past more heavily than the distant past.

The Fourier transform of the fractional derivative term is [21]

$$\mathscr{F}\{D^{\alpha}\{x(t)\}\} = (\mathrm{j}\omega)^{\alpha}\mathscr{F}\{x(t)\}, \tag{9}$$

if $x(t) = 0$ for $t < 0$. $\mathscr{F}$ denotes the Fourier transform operator. The simplicity shown in the frequency domain is an attractive feature of fractional operators, although the definition in the time domain is complicated. As seen from Eq. (5) (neglecting the non-linear terms), when $\alpha = 0$, the fractional derivative term becomes a pure stiffness term and is indistinguishable from the kx term already in the model. When $\alpha = 1$, the fractional derivative term becomes a purely viscous term of the same form as the $c\dot{x}$ term. When $0 < \alpha < 1$, the fractional derivative term resembles an intermediate status between purely elastic stiffness and purely viscous damping, which implies a contribution to both stiffness and damping.

The frequency response of the linear system with the fractional term is

$$H(\mathrm{j}\omega) = \frac{X(\mathrm{j}\omega)}{F(\mathrm{j}\omega)} = \frac{1}{-m\omega^{2} + jc\omega + a(\mathrm{j}\omega)^{\alpha} + k}. \tag{10}$$

This frequency response was evaluated with nominal values set to: $m = 2.3$ kg, $c = 5$ N s/m, $k = 283$ N/m. The results when α was set to 0.5 and a was varied from 1 to 100 are shown in Fig. 3(a). The results when a was fixed at 20 and α was varied between 0 and 1 are shown in Fig. 3(b). Recall that the fractional derivative term $aD^{\alpha}(x)$ combines both a stiffness and damping effect. When a, the coefficient of the fractional term increases, there is a greater contribution to both stiffness and damping. Thus, the amplitude at resonance goes down with increased damping and the position of the peak moves to the right with increased stiffness. As α gets closer to 1, $D^{\alpha}(x)$ becomes more like a damping term and the contribution to stiffness decreases. Therefore, the amplitude at resonance goes down and shifts to the left when α is increased.

2.3. Relaxation time constants in different models

As mentioned before, viscoelastic properties are very important to the understanding of the dynamic properties of foam materials. Since viscoelastic behavior can be characterized by relaxation and creep phenomena, it is useful to know the relaxation time constants which describe how fast the stress decays in a stress-relaxation experiment.

In the hereditary models, $1/\Re(\alpha_i)$ are essentially the system time constants, where $\Re$ denotes the real part of a complex number. To identify these material parameters, free vibration experiments were carried out in previous research [5]. The Prony method was used in the system identification of the material parameters. In one type of test, the foam–mass system was excited with an impulse and because the transient response decays very fast, it was quickly dominated by noise. Thus, only a short duration of the signal was available for analysis, and consequently only the short time

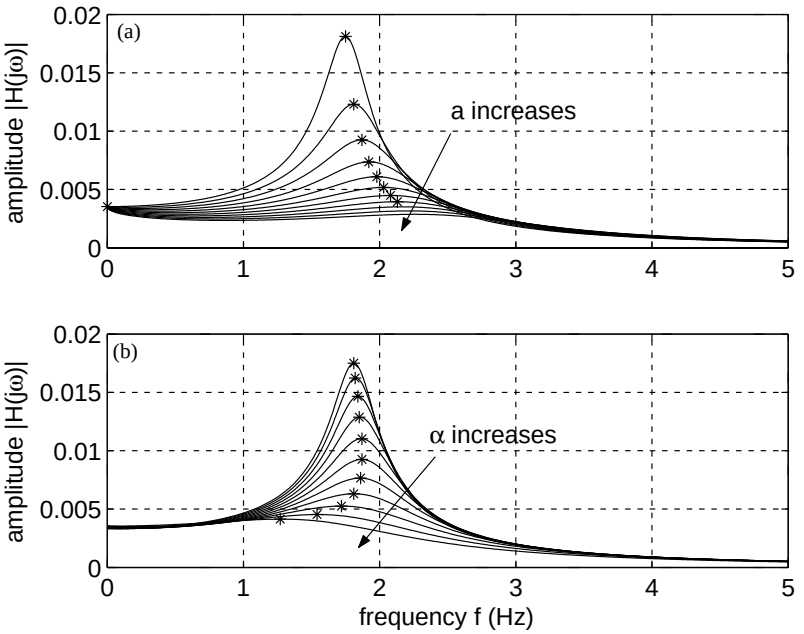

Fig. 3. The effect of variations in α and a on the behavior of frequency response of fractional derivative model. (a) $\alpha = 0.5$, a varies from 1 to 100, (b) $a = 20$, α varies from 0 to 1. Other parameters are: $m = 2.3$ kg, $c = 5$ N s/m, $k = 283$ N/m.

constants in the range from 0.07 to 0.1 s were identified. To gain information about relatively longer time constants, a quasi-static creep test was performed and the identified time constants were found to be around 20 s, 13 min and 3.5 h. There is a visible gap between these two groups of time constants and some other type of experimentation and system identification procedure may be necessary to determine whether further time constants in the range 0.1–20 s exist for the foam material.

In the hereditary model described here we have chosen $N = 2$ even though there is clear evidence that this is really too simple a model of the viscoelastic behavior. In the experiments described below, an $N = 2$ model appeared to generate reasonable approximations to the system response, perhaps indicating that for this type of test only a few of the many time constants are playing a major role in controlling the system response behavior.

Hereditary models contain a number of time constants. Plotting $|a|$ vs. the decay rate $(1/\tau_i)$ then produces a discrete relaxation spectrum. For a fractional derivative model Enelund and Lesieutre [22] hypothesized that the relaxation spectrum is continuous. In Rouse's molecular theory of viscoelasticity [23,24] an infinite number of discrete time constants are included in the viscoelastic polymer model, but the time constants are related by $\tau_n = \tau/n^2$ for $n = 1, 2, \ldots$. Bagley and Trovik [19] extended this theory to establish a link between the fractional derivative and hereditary models of stress–strain relationship for chains of polymer molecules. While tantalizingly similar in form to the polymer models, the macroscopic models of the foam behavior, as utilized in Eqs. (4) and (5), do not appear to be so easily related. Work continues in this area and more details will be presented in a future work.

2.4. Harmonic balance prediction of steady state behavior

There is no closed-form solution available for non-linear equations of motion. If the input force is harmonic, one can assume that the steady state response is periodic and an approximation to this steady state solution can be derived by using the harmonic balance method [25]. For a harmonic base excitation to the foam–mass system in Fig. 1, $x(t)$ represents the relative displacement of the rigid block with respect to the base of the fixture. The input force is $f(t) = -mG\cos(\omega_f t)$, where G is the amplitude of the input acceleration, and ω_f is its frequency.

The one-term harmonic balance solution can be assumed to be

$$x(t) = A\mathrm{e}^{\mathrm{j}\omega_f t} + \bar{A}\mathrm{e}^{-\mathrm{j}\omega_f t}, \tag{11}$$

where $A = A_r + \mathrm{j}A_i$ is the complex amplitude and $\bar{A}$ is the complex conjugate of A. From the properties of the fractional derivative operator, we know that

$$D^{\alpha}\{\mathrm{e}^{\mathrm{j}\omega_f t}\} = \omega_f^{\alpha}\mathrm{e}^{\mathrm{j}(\omega_f t + \pi\alpha/2)}. \tag{12}$$

By substituting Eq. (11) into Eq. (5), using Eq. (12) and comparing the coefficients of $\mathrm{e}^{\mathrm{j}\omega_f t}$, we get

$$-m\omega_f^2 A + \mathrm{j}c\omega_f A + kA + aA\mathrm{e}^{\mathrm{j}\pi\alpha/2}\omega_f^{\alpha} + 3k_3A^2\bar{A} + 10k_5A^3\bar{A}^2 = -mG/2. \tag{13}$$

Splitting the above equation into its real and imaginary parts, the following two equations are generated:

$$PA_r - QA_i = -mG/2, \qquad PA_i + QA_r = 0, \tag{14a, b}$$

with

$$P = -m\omega_f^2 + k + 3k_3|A|^2 + 10k_5|A|^4 + P'(\omega_f), \tag{15a}$$

$$Q = c\omega_f + Q'(\omega_f), \tag{15b}$$

where $|A|$ is the modulus of A. $P'(\omega_f)$ and $Q'(\omega_f)$ are given by

$$P'(\omega_f) = a\omega_f^{\alpha}\cos\left(\frac{\pi}{2}\alpha\right), \qquad Q'(\omega_f) = a\omega_f^{\alpha}\sin\left(\frac{\pi}{2}\alpha\right).$$

Simpler expressions can be obtained if Eq. (13) is multiplied by $\bar{A}$ and then split into its real and imaginary parts which yields

$$P|A|^2 + mGA_r/2 = 0, \qquad Q|A|^2 - mGA_i/2 = 0. \tag{16a, b}$$

An equation for $|A|$ can also be obtained by squaring and adding Eq. (16a,b) giving

$$\begin{aligned} &100k_5^2|A|^{10} + 60k_3k_5|A|^8 + \{20(-m\omega_f^2 + k + a\omega_f^{\alpha}\cos(\pi/2\alpha))k_5 + 9k_3^2\}|A|^6 \\ &+ 6k_3\{-m\omega_f^2 + k + a\omega_f^{\alpha}\cos(\pi/2\alpha)\}|A|^4 + \{(-m\omega_f^2 + k + a\omega_f^{\alpha}\cos(\pi/2\alpha))^2 \\ &+ (c\omega_f + a\omega_f^{\alpha}\sin(\pi/2\alpha))^2\}|A|^2 - m^2G^2/4 = 0. \end{aligned} \tag{17}$$

This equation is a fifth order polynomial in $|A|^2$. Only positive roots are valid since $|A|$ is always positive. Once the amplitude of A is known, the phase of the harmonic approximation to the

periodic solution can be calculated from

$$\angle A = \tan^{-1}(A_i/A_r) = \tan^{-1}\left\{\frac{Q}{-P}\right\}. \tag{18}$$

The response can be predicted by using the above two equations if the material parameters are known.

For the hereditary model, an equation similar to Eq. (13) can be derived [6]:

$$-m\omega_f^2 A + \mathrm{j}c\omega_f A + kA + 3k_3 A^2 \bar{A} + 10k_5 A^3 \bar{A}^2 - k\left(\frac{a_1}{\alpha_1 + \mathrm{i}\omega_f} + \frac{a_2}{\alpha_2 + \mathrm{i}\omega_f}\right)A = -mG/2. \tag{19}$$

Then, mirroring the derivation of Eqs. (14) and (16), the structure of the equations for the hereditary model is seen to be the same, but $P'(\omega_f)$ and $Q'(\omega_f)$ are now given by

$$P'(\omega_f) = -k\left(\frac{\alpha_r a_r + \alpha_i a_i + \omega_f a_i}{\alpha_r^2 + (\omega_f + \alpha_i)^2} + \frac{\alpha_r a_r + \alpha_i a_i - \omega_f a_i}{\alpha_r^2 + (\omega_f - \alpha_i)^2}\right),$$

$$Q'(\omega_f) = -k\left(\frac{\alpha_r a_i - \alpha_i a_r - \omega_f a_r}{\alpha_r^2 + (\omega_f + \alpha_i)^2} + \frac{-\alpha_r a_i + \alpha_i a_r - \omega_f a_r}{\alpha_r^2 + (\omega_f - \alpha_i)^2}\right).$$

3. System identification

The system identification of the material parameters is based on Eqs. (14) or (16) and it is assumed that A_r and A_i are known for a set of values of ω_f. Denoting Eqs. (14a,b) (or equivalent equations in hereditary model) or Eqs. (16a,b) as $F_1(\omega_{fi})$ and $F_2(\omega_{fi})$, respectively, the estimation for the material parameters (c, k, k_3, k_5, a, α) can be performed by minimizing the error function:

$$\mathscr{E} = \sum_{i=1}^{M} (|F_1(\omega_{fi})|^2 + |F_2(\omega_{fi})|^2), \tag{20}$$

where the ω_{fi} are the frequencies at which the steady state response is evaluated.

The minimization of this cost function results in a set of non-linear equations that need to be solved to obtain the system parameters. The program 'lsqnonlin' in Matlab was used to find the solution to these non-linear equations. This program is based on the trust region method in which the cost function is approximated by a simpler function in the neighborhood (so called 'trust region') of the current system parameters. After the trust region is determined with the aid of a preconditioned conjugate gradient process, the new step is calculated and the system parameters are modified [26]. This algorithm is sensitive to many set-up parameters including the bounds for the parameters, the error tolerances, and the scaling of the parameters. Therefore, lower bounds and upper bounds were set for all the system parameters. In particular, c and k were restricted to be positive since negative values are not physically feasible. α was set to be between 0 and 1, and a was allowed to be any value when c was included as a parameter in the model. The reason for allowing a to be a negative value is discussed in Section 4.3. k_3 was limited to be a negative value and k_5 was limited to be a positive value. These limits were based on our understanding of the

system gained from fitting the hereditary model to the experimental data. The system parameters were also scaled to be of similar magnitudes in order to avoid ill conditioning. In addition, a Jacobian matrix was provided to save the number of function evaluations. The option of 'PrecondBandWidth' was set to infinity in order to fit the program to our case which does not have many parameters to estimate. The stopping criteria in the program are satisfied when the norm of the cost function or the difference between parameter values obtained in the last two steps is less than the tolerances set to 10^{-20} and 10^{-18}, respectively. The program indicates whether convergence has been achieved.

Another way of solving this problem is to use a sub-optimal method introduced in Ref. [6]. If α is known, the estimation of the remaining material parameters in Eq. (14) or (16) is a simple linear optimization problem. This is true for both the hereditary and the fractional derivative models. Motivated by the success of using this approach with the hereditary model, a fine grid of possible values of α is formed from 0 to 1, and the rest of the fractional derivative model parameters are estimated by using a linear least-squares formulation. Then the error $\mathscr{E}$ can be calculated for every choice of α. The selected α and the other parameters corresponding to the minimum value of $\mathscr{E}$ are the estimates of the material parameters. The grid can be further refined around the minimum to improve the accuracy of the solution.

For the hereditary model, the sub-optimal method was used to estimate the system parameters. Similar results can be obtained by using the direct non-linear estimation from 'lsqnonlin' program. For the fractional model, the 'lsqnonlin' program was almost always used. The sub-optimal approach was also used for this problem to examine the error surface when there were problems with convergence.

When applying these system identification techniques, there are several issues that must be addressed. These include the choice of the cost function, the frequency resolution and the amount of data. These are discussed below.

3.1. Choice of the cost function

There are two sets of equations that can be used as cost functions for identification: Eqs. (14a,b) or Eqs. (16a,b). The second set of equations is obtained by multiplying the original equation with $\bar{A}$, which is the complex conjugate of the amplitude of the response. Ideally, if the model is perfect for the system under investigation, these equations should have a unique solution and this multiplication by a constant should not affect the estimation results. However, because of noise and model imperfections, different predictions might be expected from the two cost functions since the multiplication by $\bar{A}$ effectively weights the cost function more strongly at points where A is large.

To investigate this effect, response data were simulated using Eqs. (17) and (18) with realistic parameters that give a reasonable fit to experimental data at 50% compression and a -0.25 mg N base excitation. Uniformly distributed zero-mean white noise was added to $A_r(\omega_j)$ and $A_i(\omega_j)$ separately. The width of the distribution was selected to be a percentage of the peak value of $A_r(\omega_j)$ and $A_i(\omega_j)$. Noise levels varied from 0.1% (60 dB) to 1.9% (34 dB) of the peak value. This ranged from slightly worse to slightly better than the noise conditions in the experiment. By adding noise in this way, a better signal to noise ratio was obtained in the peak region which is the situation in the experiment. The material parameters were estimated by using the direct non-linear

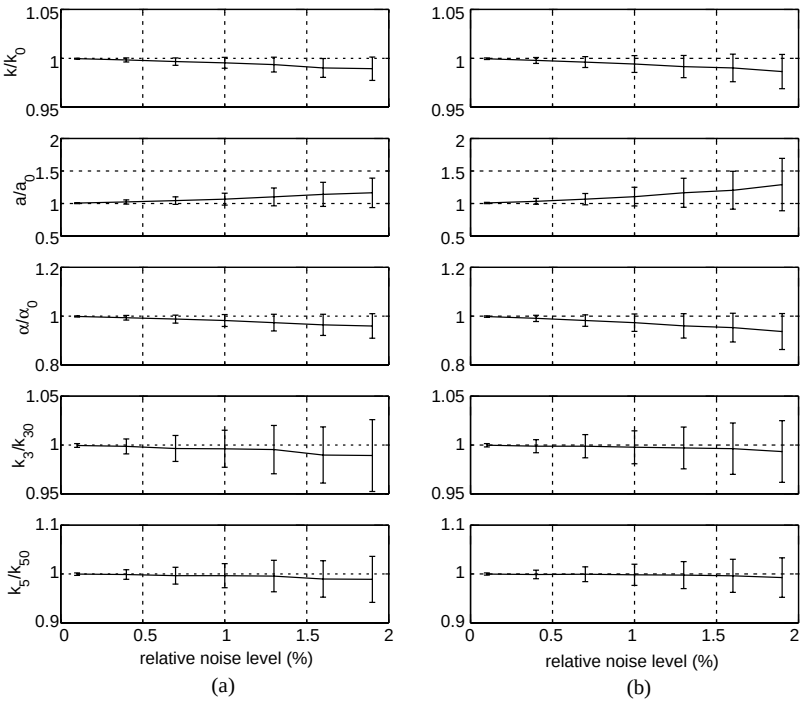

Fig. 4. Normalized mean values and standard deviations of estimates of material parameters from 1000 tests in the fractional derivative model with data at 50% compression, $G = -0.25$ mg N and at different noise levels. (a) Estimates from formulation multiplied by $\bar{A}$. (b) Estimates from formulation not multiplied by $\bar{A}$. The variables with the subscript '$_0$' represent the true values of the parameters.

optimization algorithm on data from 1000 simulations at each noise level, and using the two types of cost functions. The error bars represent the mean estimation $\pm$ the standard deviation of the estimates divided by the true value. The viscous damping parameter was not include here; this omission is discussed in Section 4.3.

We can see from Fig. 4 that at low noise levels, the predictions are very close to the original value for both cost functions. As expected, the bias and variance of the estimates increase with increasing noise. At higher noise levels, the cost function that includes multiplication by $\bar{A}(\omega_f)$ gives slightly better estimates of k, a and α. Similar patterns were observed from hereditary model simulations. The data near the peak region, which have a better signal-to-noise ratio, are weighted more than those far away from the peak in the response. Thus the emphasis of this portion of data should help in the estimation of parameters. In light of this, the cost function with the multiplication with $\bar{A}(\omega_f)$ is used in the analysis and estimation from the experimental data.

3.2. Frequency resolution of data

The data obtained from experiments need to have sufficient resolution in frequency to capture the essential features of the response. To study the effect of the frequency resolution on the estimates of the material parameters, simulations similar to those described in Section 3.1 for the fractional derivative model at 50% compression and $G = -0.25$ mg N were conducted. Again, the

viscous c term was not included in the simulation because its inclusion tends to increase the variance of the parameter estimates. Uniformly distributed noise at a level of 1.9% of the largest amplitude at the finest resolution was added to the simulation data. The frequency range spans from 2 to 8 Hz. The frequency resolution at each level is twice as that for the previous level, i.e., level 1 has a resolution of 0.5 Hz, level 2 has a resolution of 0.25 Hz and so on. Level 5 has a very fine frequency resolution of 0.03125 Hz. Note that the upper limit constraint ($\alpha < 1$) was not applied to α during the optimization procedure in this case; this issue is discussed in more details in Section 4.3.

The normalized mean values and standard deviations of the estimated parameters from 1000 simulations are shown in Fig. 5(a) for the case of $\alpha = 0.9$. It is observed that the standard deviations of the estimates for system parameters decrease as the resolution gets finer. This could be because the better resolution provides more information on the behavior of the system, or because more data points are taken with a higher resolution in the fixed frequency range (it is referred to as the 'n effect' in Fig. 5). With more data, it would be expected that the standard deviation of the estimates becomes smaller.

To remove the effect of taking more data when using a higher resolution, several data sets from low resolution simulations were combined in the estimation. By doing so, 200 points were used at each resolution level. The results of the estimations are shown in Fig. 5(b). It can be seen that there appears to be only small change in the mean values and standard deviations of the estimated

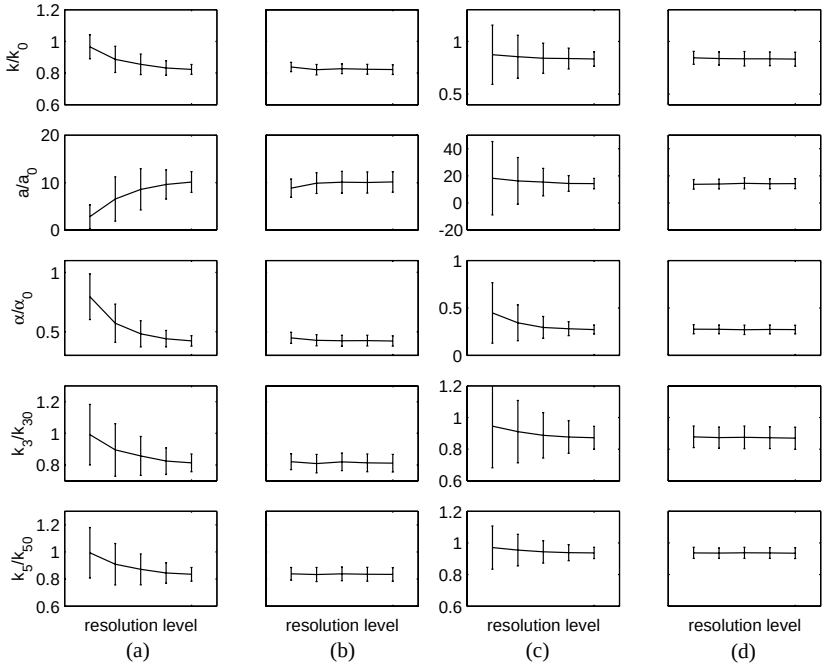

Fig. 5. Normalized mean values and standard deviations of estimated parameters at different resolution levels in the fractional derivative model for data at 50% compression level and $G = -0.25$ mg N. (a) More data used when resolution increases. $\alpha_0 = 0.9$. (b) Same number of data points (200) at all resolutions. $\alpha_0 = 0.9$. (c) More data used when resolution increases. $\alpha_0 = 0.5$. (d) Same number of data points (200) at all resolutions. $\alpha_0 = 0.5$. The variables with the subscript '$_0$' represent the true values of the parameters.

parameters as the resolution level increases. It should be noted, however, that a resolution of 1 Hz produced extremely poor results (not shown) because at this resolution very little detail in the frequency response is retained.

As illustrated in Fig. 5(a), lower variance estimates for the viscoelastic parameters a and α were found at the lowest frequency resolution of 0.5 Hz, which is considered to be the worst case in terms of system information. To investigate this problem, similar simulations were conducted for different values of α. It was observed that this problem only happens when α is close to 1. The results for $\alpha = 0.5$ are shown in Fig. 5(c). It can be seen that the standard deviations of estimates decrease as the frequency resolution increases. No substantial changes can be observed in either the mean values or the standard deviations of estimates when the number of data points are the same at each resolution level as shown in Fig. 5(d). It is not very clear at this moment why the cases when α is close to 1 lead to counterintuitive results in the variance of the estimated parameters at frequency resolution of 0.5 Hz and the problem is currently being investigated.

There are also interesting bias effects: with a few exceptions, when more data points are used the bias changes, often leading to larger bias with the increased number of data points. Simulations with different numbers of data points were carried out at a fixed frequency resolution level of 0.5 Hz for $\alpha = 0.5$ and 0.9. At each level in these simulations, the number of data points is twice as that of the previous level, i.e., level 1 has 14 data points, level 2 has 28 data points, obtained by combining two data sets of the previous level, and so on. Uniformly distributed noise as described in previous simulations is added to the simulation data. The results of estimation are shown in Fig. 6 and again it is observed that the bias of the estimates increases as the number of data points increases and this effect is more pronounced when α approaches 1.

The distributions of the normalized parameter estimates for the case of $\alpha = 0.9$ are shown in Fig. 7. The probability density functions of the estimated parameters, together with a Gaussian probability density function, generated by using the estimated mean and standard deviation of the estimates, were estimated from 30,000 simulations. The vertical line represents the true normalized value 1. The results reflect the same shift in bias shown in Fig. 6, but in addition, the results clearly indicate the complexity of the statistics of the parameter estimates. As seen from the figure, the probability density functions become Gaussian as the number of data points used in the estimation increases.

From this investigation we can conclude that increasing the resolution above 0.25 Hz (the resolution used in the experimental work reported in the next section) results in only small improvements in the estimates. The estimates deteriorate significantly if the resolution is below 0.5 Hz. As noise decreases, bias errors decrease, but bias was in general worse when we used more data points in the estimation. Thus in the case where several data sets are available, it is better to average sets at each frequency (to reduce noise) before proceeding to the estimation. Using all original noisy data simultaneously in the estimation appears to lead to an increase in parameter bias.

4. Identification from experiments and simulations

The foam–mass system shown in Fig. 1 was harmonically excited through motion of its base that was attached to an MTS hydraulic shaker, and the steady state responses were recorded at

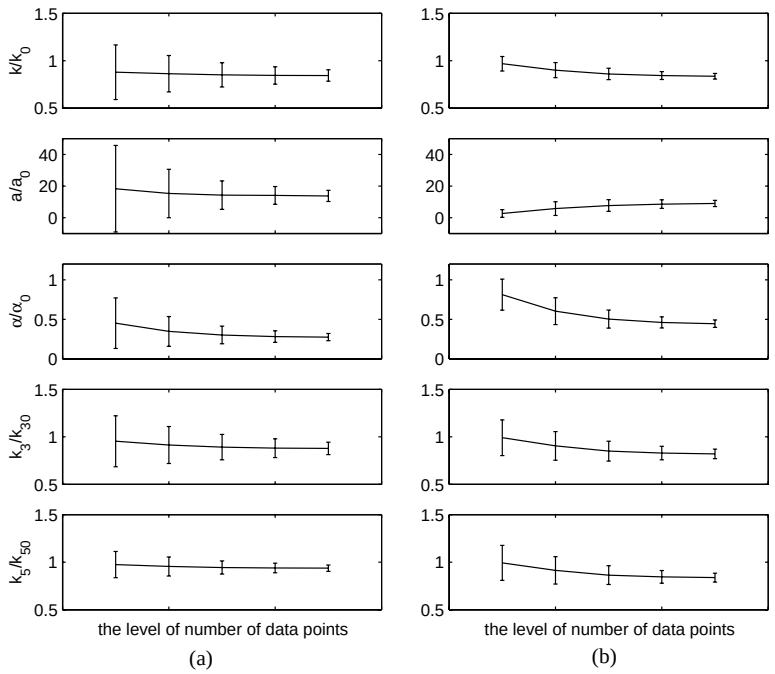

Fig. 6. Effect of number of data points on the normalized mean values and standard deviations of the estimated parameters in the fractional derivative model for data at 50% compression level and $G = -0.25$ mg N. (a) $\alpha_0 = 0.5$ (1:20 data points; 2:40 data points and so on). (b) $\alpha_0 = 0.9$ (1:14 data points; 2:28 data points and so on). The variables with the subscript '$_0$' represent the true values of the parameters.

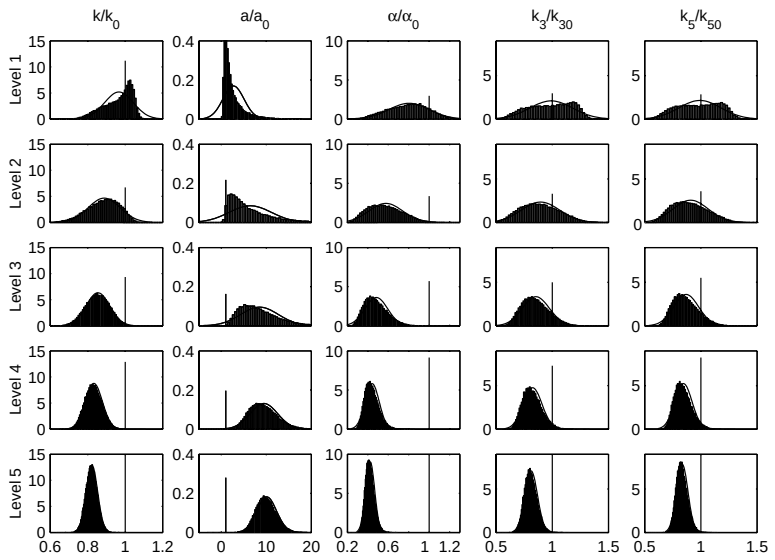

Fig. 7. Probability density functions of the estimated parameters at different levels of number of data points in the fractional derivative model for data at 50% compression level and $G = -0.25$ mg N. The results were normalized with respect to the true values. $\alpha_0 = 0.9$. The variables with the subscript '$_0$' represent the true values of the parameters.

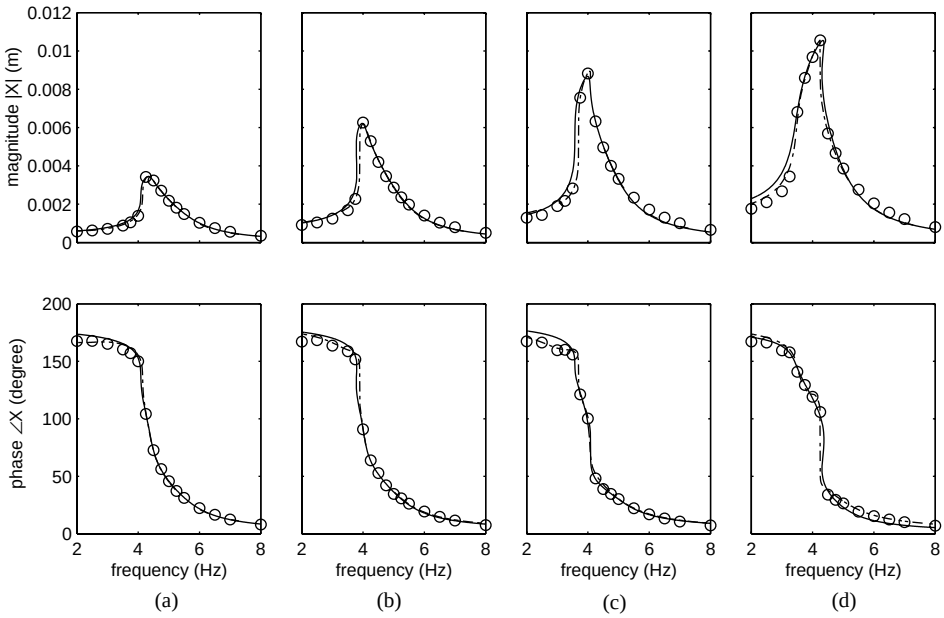

Fig. 8. Fractional and hereditary model predictions and measured responses for different excitation levels at 30% compression. (a) $G = -0.10$ mg N, (b) $G = -0.15$ mg N, (c) $G = -0.20$ mg N, (d) $G = -0.25$ mg N. o, measured data; —, response predicted by the fractional derivative model; ,-.-, response predicted by the hereditary model.

four excitation levels (0.1, 0.15, 0.2, and 0.25 mg N) and at three compression levels (30%, 40% and 50%). The foam sample used is a 7.62 cm × 7.62 cm × 7.62 cm cube. The masses that were used to obtained the desired three compression levels are 2.29, 2.86, and 3.38 kg, respectively. Since the foam is a complex viscoelastic material whose static properties are different from the dynamic properties, the test was performed very carefully in order to achieve consistent measurements. The foam was first pre-loaded and several hours were allowed for the foam to settle down to its static equilibrium position. Before the measurement, dynamic exercise was conducted for 3 h to allow the foam to reach the true equilibrium compression level and then the steady state response was recorded after steady state behavior had been achieved at each frequency of excitation.

There are several practical issues in the experiment that affect the model parameter estimates. The top plate sitting on the foam (see Fig. 1) may have rocking motion if the foam is not homogeneous and of constant thickness or the four posts are not perfectly aligned. The fixture may also introduce dry friction that is not considered in the models. The measurement noise is small in this case since the signal-to-noise ratio in the single frequency excitation experiment is relatively high. The details concerning the experimental issues are discussed in detail in Ref. [27].

4.1. Parameter estimation and prediction from experimental data

System identification procedures based on both models were applied to the experimental data. The frequency range of the experimental data is from 2 to 8 Hz. Data sets used had a resolution of

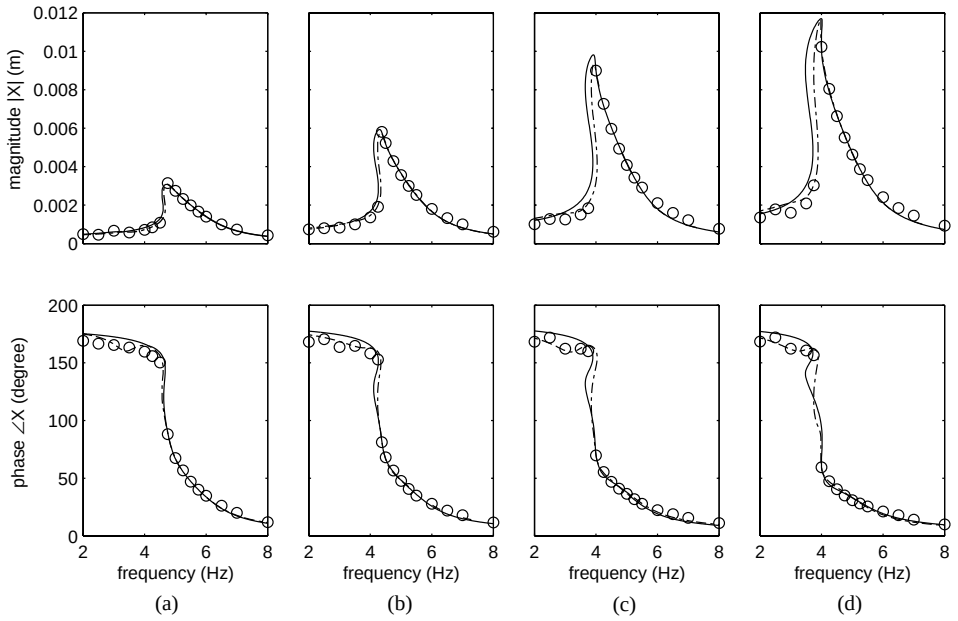

Fig. 9. Fractional and hereditary model predictions and measured responses for different excitation levels at 50% compression. (a) $G = -0.10$ mg N, (b) $G = -0.15$ mg N, (c) $G = -0.20$ mg N, (d) $G = -0.25$ mg N. o, measured data; —, response predicted by the fractional derivative model; ,-.-, response predicted by the hereditary model.

0.5 Hz below 3.5 Hz and above 5.5 Hz, and a resolution of 0.25 Hz in the range from 3.5 and 5.5 Hz. The parameters of the fractional derivative model were estimated directly by using the non-linear optimization method while the sub-optimal method was used for the hereditary model estimation. The predictions at 30% and 50% compression level from both the models together with the measured responses are shown in Figs. 8 and 9, respectively. The estimated parameters at the 50% compression level are listed in Tables 1 and 2 for the fractional derivative model and the hereditary model, respectively.

From the results shown in Table 1, it can be seen that for the fractional derivative model there is much variation in the estimates of parameters from one level to another. The magnitudes of the non-linear stiffness coefficients k_3 and k_5 decrease as the input amplitude increases. The same pattern for k_3 and k_5 is also observed in the hereditary model, as shown in Table 2. The estimates of k_3 and k_5 from the two types of models are very close to each other for the same level of excitation. The estimates of the viscoelastic parameters α and a in the hereditary model are also seen to vary considerably with the input amplitude. The estimates of c and k remain relatively stable for all input amplitudes in the hereditary model.

As shown in Figs. 8 and 9, the two models provide fairly good predictions in both amplitude and phase at low input acceleration for both of the compression levels. Only at higher input levels (0.20 and 0.25 mg) does the prediction from the fractional derivative model not match the experimental data very well below the resonance region. The hereditary model does a reasonably good job even at these high input levels. This may be an indication of the inadequateness of the fractional derivative model for high compression levels and input excitations.

Table 1
Estimated fractional derivative model parameters at different input levels for 50% compression

G (N)	−0.1 mg	−0.15 mg	−0.2 mg	−0.25 mg
c (N s/m)	14.0	595	26.3	1317
k (N/m)	0.181×10^3	3.98×10^3	3.53×10^3	3.38×10^3
(Constrained)	(4.10×10^3)	(3.71×10^3)	(3.19×10^3)	(3.12×10^3)
(Unconstrained)	(4.10×10^3)	(3.96×10^3)	(3.43×10^3)	(3.40×10^3)
k_3 (N/m^3)	-8.11×10^7	-2.70×10^7	-1.05×10^7	-0.88×10^7
(Constrained)	(-8.08×10^7)	(-2.62×10^7)	(-1.02×10^7)	(-0.85×10^7)
(Unconstrained)	(-8.08×10^7)	(-2.72×10^7)	(-1.08×10^7)	(-0.90×10^7)
k_5 (N/m^5)	118×10^{10}	12.89×10^{10}	2.04×10^{10}	1.39×10^{10}
(Constrained)	(118×10^{10})	(12.67×10^{10})	(1.98×10^{10})	(1.35×10^{10})
(Unconstrained)	(118×10^{10})	(12.96×10^{10})	(2.08×10^{10})	(1.41×10^{10})
a (N/m$^\alpha$)	3.81×10^3	-0.60×10^3	-0.08×10^3	-1.32×10^3
(Constrained)	(32.27)	(15.79)	(14.11)	(14.19)
(Unconstrained)	(32.27)	(7.16)	(6.25)	(5.55)
α	0.019	0.992	0.523	0.996
(Constrained)	(0.84)	(1.00)	(1.00)	(1.00)
(Unconstrained)	(0.84)	(1.26)	(1.28)	(1.33)

The parameters in parentheses are estimates from the model without the viscous damping term. 'Constrained' and 'unconstrained' correspond to the results from the optimization procedures with and without applying the upper limit to α respectively.

Table 2
Estimated hereditary model parameters at different input levels for 50% compression

G (N)	−0.10 mg	−0.15 mg	−0.20 mg	−0.25 mg
c (N s/m)	18.0	20.2	20.1	19.9
k (N/m)	4.18×10^3	3.65×10^3	3.12×10^3	3.03×10^3
k_3 (N/m^3)	-8.12×10^7	-2.67×10^7	-1.11×10^7	-8.99×10^6
k_5 (N/m^5)	110×10^{10}	11.9×10^{10}	1.94×10^{10}	1.31×10^{10}
a (s^{-1})	-0.099 ± 0.355i	-0.272 ± 0.037i	-0.469 ± 0.232i	-0.467 ± 0.162i
α (s^{-1})	2.74 ± 21.8i	3.62 ± 24.8i	3.21 ± 21.68i	3.58 ± 22.0i

4.2. Relationship between hereditary and fractional derivative models

It was found that the fractional derivative model appeared to have less flexibility in modelling the experimental data. To examine this further, the response was simulated with one type of model and a model of the other type was identified with this simulated data. At low levels of compression (30%), the estimated model responses were close to the simulated responses

regardless of which model was used to simulate the response, as shown in Fig. 10. At higher compression levels (50%) and at high levels of excitation the hereditary model fit the fractional model response well, but not vice versa; this is illustrated in Fig. 11.

In Bagley and Torvik's derivation [19] of the fractional derivative polymer model from a hereditary-type model with a large number of time constants, it appeared that the fractional derivative model was a compact description that encompassed a wide variety of time constants. The derivation was based on a fixed relationship between the time constants ($\tau_n = \tau/n^2$) which leads to a fractional order of $1/2$. If this were the case here, we would expect that a large number of exponential terms in the kernel of the viscoelastic model would be required to model the data from fractional derivative model. However, this is clearly not the case for this system and this type of excitation. While there are two hereditary kernel terms, they are a complex conjugate pair and thus only one decay rate ((time constant)$^{-1}$) is associated with this pair of terms. It appears that only one time constant is sufficient to reproduce the fractional derivative model behavior. This may be an indication that the relationship between the time constants is not as straightforward as the one used in the polymer model derivation, or that under this excitation very few of the infinite number of time constants play a role in the response.

4.3. The role of the viscous damping term

The estimates of the linear parameters, including the viscous damping coefficient c and the stiffness coefficient k, vary considerably for different input amplitudes in the fractional model.

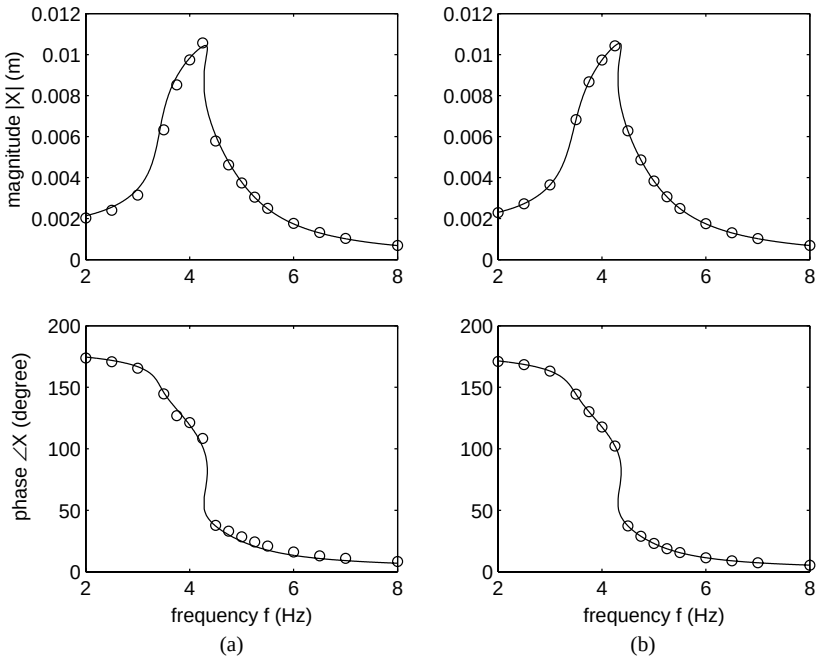

Fig. 10. Estimated model predictions of simulated data at 30% compression and $G = -0.25$ mg N. (a) Hereditary simulation and estimated fractional derivative model predictions. (b) Fractional derivative simulation and estimated hereditary model predictions. o, simulated data; —, predicted response.

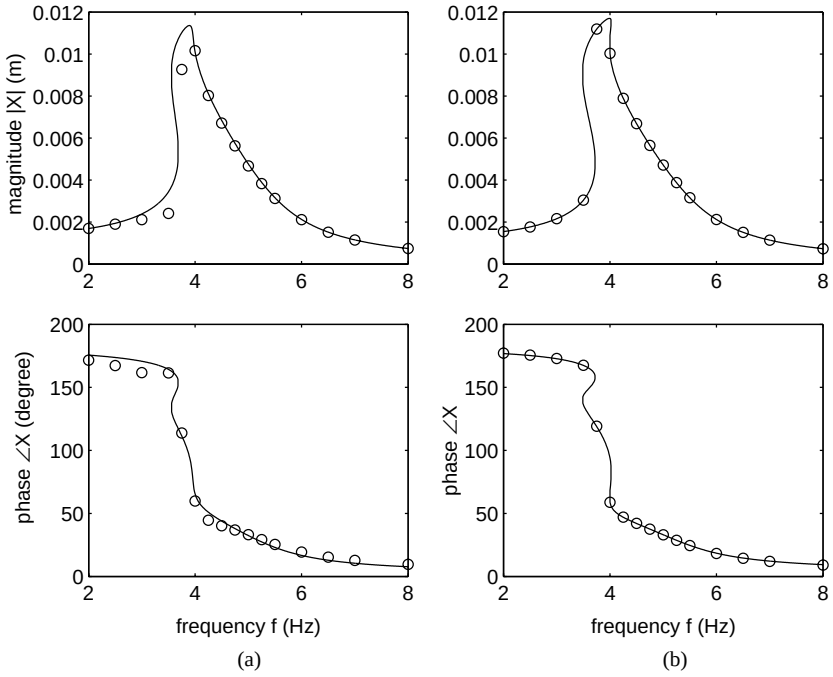

Fig. 11. Estimated model predictions of simulated data at 50% compression and $G = -0.25$ mg N. (a) Hereditary simulation and estimated fractional derivative model predictions. (b) Fractional derivative simulation and estimated hereditary model predictions. o, simulated data; —, predicted response.

Recall that the fractional derivative term $aD^{\alpha}x(t)$ affects both stiffness and damping. Whether the linear velocity proportional damping term is necessary in this model is an interesting question. System identification and the prediction of response were carried out for the non-linear fractional derivative model for the case when c is not included. As shown in Fig. 12, the predicted response for 50% compression level data is hardly affected by the exclusion of the c term. The results for other compression and input levels exhibit similar behavior. The details of these results are omitted here. This indicates that c is a redundant variable in the fractional derivative model and that its presence may cause the other parameters to vary significantly because many combinations of the terms result in almost identical predictions.

The estimated parameters for the fractional derivative model without the c term for 50% compression are shown in Table 1 in parentheses (corresponding to 'constrained' case). It can be seen that the estimates of the non-linear parameters k_3 and k_5 remain very close to the previous results. The variations in the other parameters (k, a and α) are smaller when c is not included in the model. The value of stiffness k decreases with the increased excitation level. a also exhibits a slightly decreasing trend with increasing excitation level. Note that the fractional order α becomes 1 for the higher excitation levels, which indicates that the fractional model effectively evolves to a spring–damper model at these levels. This result may also be explained by the fact that α was constrained to be equal to or less than 1 in the optimization process. The parameters were re-estimated without this constraint and the results are also shown in Table 1 (corresponding to the

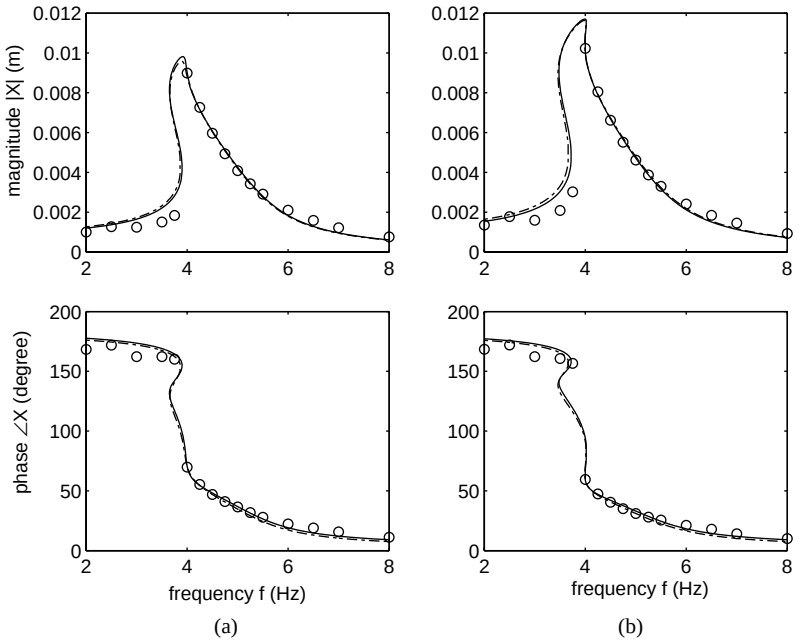

Fig. 12. Measured and predicted responses from the fractional derivative model with and without the viscous damping term. (a) 50% compression level and $G = -0.20$ mg N, (b) 50% compression level and $G = -0.25$ mg N. o, measured response; —, response predicted with c, -.-, response predicted without c.

'unconstrained' case). It can be seen that if α is not constrained, the optimized values for α are usually between 1 and 2, which represents a term between a viscous damping and an inertia term. However, the predicted responses are very close to the results when α was limited between 0 and 1. This is due to the insensitivity of the function used in the identification algorithm to the small changes in the parameters a and α, and this is another indication of the insufficiency of the structure of the fractional derivative model to model responses at high compression and excitation levels.

To investigate the problem of the redundancy of the viscous damping term further, simulations were carried out at different noise levels. Uniformly distributed noise at levels from 0.1% to 1.9% with respect to the peak value of the response, as described earlier, was added. At each noise level, 1000 simulations were conducted and the normalized mean value and standard deviation of the estimated parameters before and after c was removed were calculated. The results are shown in Fig. 13. It is very clear that after c is removed, the estimation of the material parameters is more accurate and that it is therefore better to compare the variation of parameters under different experimental conditions with c excluded.

Similarly one might ask, whether the viscous damping term is implicitly incorporated in the viscoelastic kernel of the hereditary model? When the direct non-linear estimation procedure was used to identify the system parameters of the hereditary model without the c term, difficulties were encountered in obtaining converged estimates of the system parameters. It is suspected that the

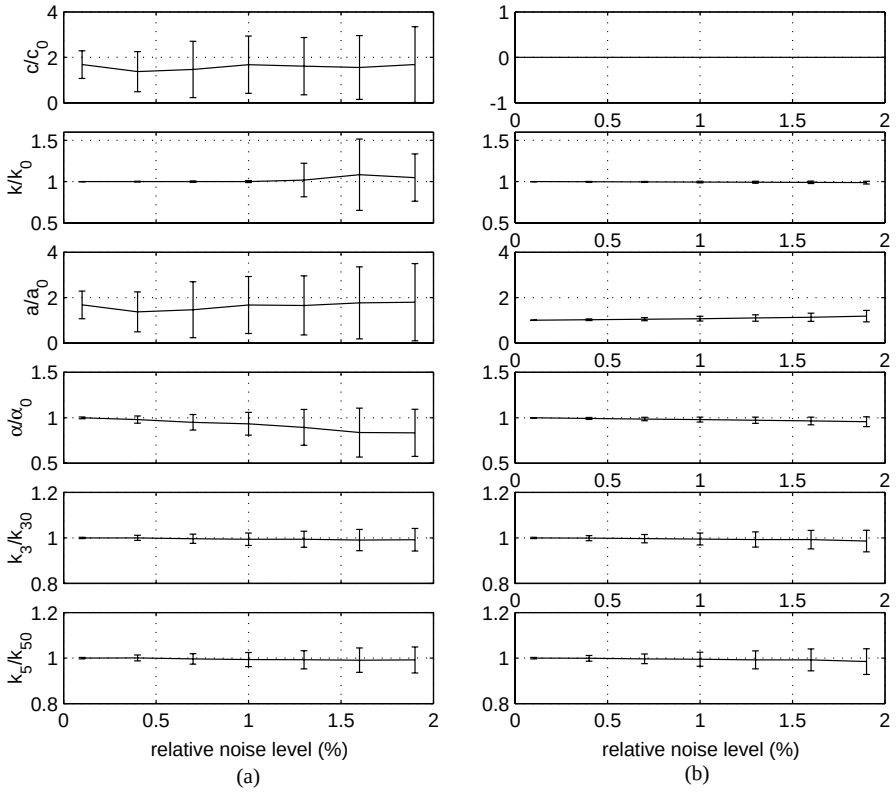

Fig. 13. Fractional derivative model estimates with and without the viscous damping term. The normalized mean value and standard deviation of parameters estimated from 1000 simulations for 50% compression with −0.25 mg input level are shown. (a) Estimates based on formulation with c. (b) Estimates based on formulation without c. The variables with the subscript '$_0$' represent the true values of the parameters.

error surface is very flat in the parameter space when c is excluded from the model and that it is difficult to find the minimum for this case. Therefore, the sub-optimal identification procedure without the c term was used to investigate the error surface properties. A grid of values of α_r and α_i was specified and the error in the estimation at each combination of α_r and α_i was plotted. This error surface is very flat and does not have a strong minimum or, if a minimum does exist, it is highly localized and the grid utilized is not fine enough to detect it. The level curves of the error surface for determination of the viscoelastic parameters α_r and α_i is shown in Fig. 14(a). It can be seen that the dark region, which represents the location of the minimum, is very flat and that it extends to the region where the real part of α and the imaginary part of α are quite large. A minimum can usually be found in the extended flat region if the error surface is zoomed in, as shown in Fig. 14(b). Around the minimum is an insensitive region where the cost function is affected very little by the variations in α_r and α_i. This is perhaps an indication of the insufficiency of the model structure.

The predictions of the response based on the estimated parameters when c is excluded from the hereditary model are shown in Figs. 15 and 16 for the 50% and 30% compression levels,

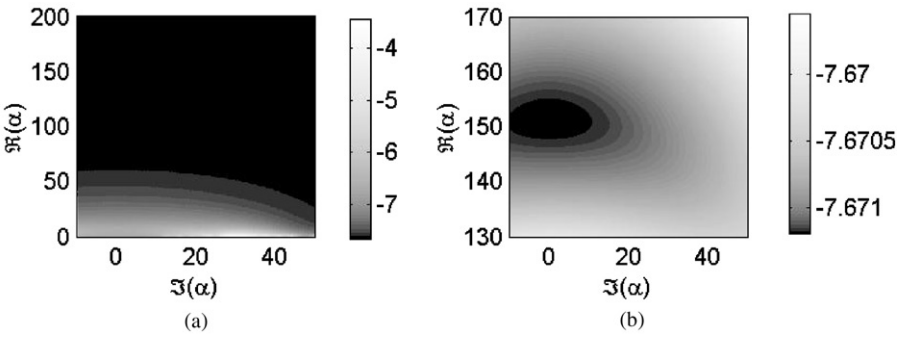

Fig. 14. Level curves of the error surface ($\ln|\mathscr{E}|$) for the hereditary model sub-optimal estimation for 50% compression experimental data at $G = -0.25$ mg N. (a) The global error surface, (b) The local error surface around the minimum. The viscous damping term is not included in the model.

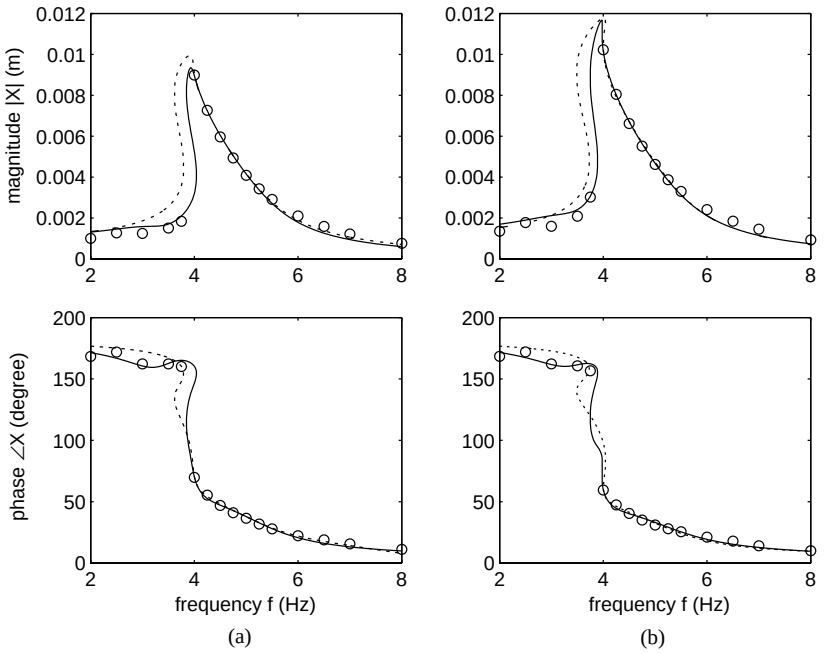

Fig. 15. Measured and predicted response from hereditary model with and without the c term. (a) 50% compression level and $G = -0.20$ mg N, (b) 50% compression level and $G = -0.25$ mg N. o, measured responses; —, response predicted with c in the model; ⋯ response predicted without c in the model.

respectively. It can be seen that the predictions from the model without the c term do not match the experimental data as well as those from the model with the damping term c at the higher compression level (50%). However, at the lower compression level (30%), the differences become less significant, as illustrated in Fig. 16. A possible explanation of this observation is that the foam's behavior is more complicated at higher compression levels and input amplitudes, and the

additional damping term helps model this behavior. This may also explain why the fractional derivative model cannot fit the experimental data very well at these high compression and input levels. At the same time, because of the characteristics of this fractional derivative term, even an explicit damping term in the form of viscous damping does not help the estimation. This indicates that some other damping mechanism needs to be included to fully represent the behavior of foam materials. Patten et al. [7] introduced a quadratic non-linear damping model for seat cushion. It was assumed that the dissipation of energy in foam under dynamic load is due to the fluid flow loss introduced by the fluid contained in foam. The model prediction matched well with the measured frequency response of the mass–seat system at various input levels. The quadratic damping model may help improve the performance of the fractional derivative model at high compression and excitation levels. In addition, the micro-structural models [28,29] showed that when foam is highly compressed, the material struts that form the matrix of the foam may rub against each other and that the dry friction should be considered for the determination of energy loss. Therefore, incorporating an internal dry friction model may also be an option for the improvement of foam models.

4.4. A further note on the fractional derivative model

To explore the performance of the fractional derivative models further, the full fractional derivative model represented by Eq. (3) was incorporated into the foam–mass system, resulting in

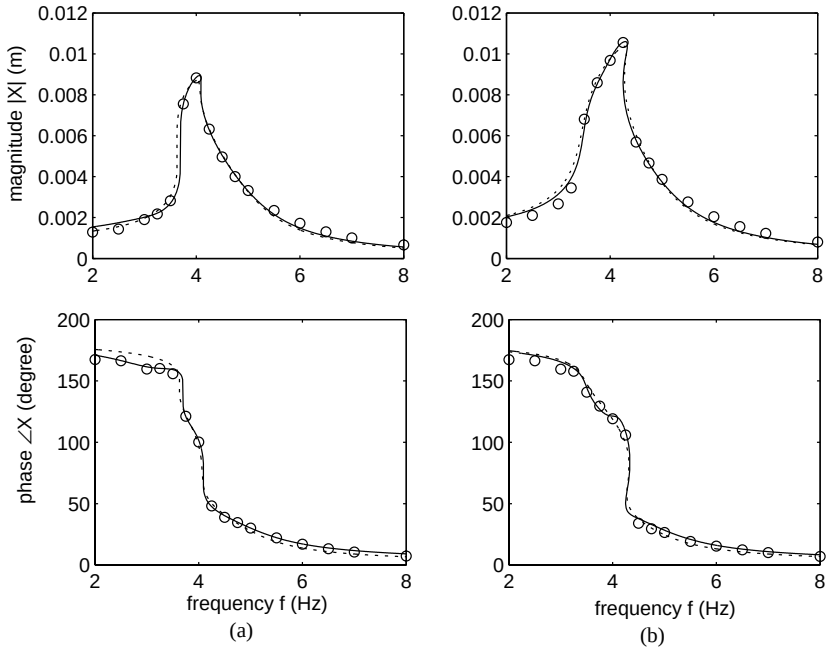

Fig. 16. Measured and predicted response from the hereditary model with and without the c term. (a) 30% compression level and $G = -0.20$ mg N, (b) 30% compression level and $G = -0.25$ mg N. o, measured data, —, response predicted with c in the model; ⋯, response predicted without c in the model.

the equation of motion

$$m\ddot{x} + k_3x^3 + k_5x^5 + F_d = f(t), \tag{21}$$

where F_d is the restoring force represented by the fractional derivative model and is given by the solution to

$$F_d + a_1D^\alpha F_d(t) = kx + a_2D^\alpha x(t). \tag{22}$$

Here, the two α's are chosen to be the same and a_1 and a_2 are the coefficients of the two fractional derivative terms. The viscous damping term is not included again for the reasons discussed in Section 4.3. This model will be referred to as the two-term fractional derivative model while the previous model will be called the one-term fractional derivative model.

Assuming the one-term harmonic balance solution, the above two equations lead to the same two equations, Eqs. (15) and (16), except that the functions $P'(\omega_f)$ and $Q'(\omega_f)$ are now given by

$$P'(\omega_f) = \frac{(a_2\omega_f^\alpha \cos(\frac{\pi}{2}\alpha) + k)(1 + a_1\omega_f^\alpha \cos(\frac{\pi}{2}\alpha)) + a_1a_2\omega_f^{2\alpha} \sin^2(\frac{\pi}{2}\alpha)}{1 + 2a_1\omega_f^\alpha \cos(\frac{\pi}{2}\alpha) + a_1^2\omega_f^{2\alpha}},$$

$$Q'(\omega_f) = \frac{a_2\omega_f^\alpha \sin(\frac{\pi}{2}\alpha)(1 + a_1\omega_f^\alpha \cos(\frac{\pi}{2}\alpha)) - (a_2\omega_f^\alpha \cos(\frac{\pi}{2}\alpha) + k)a_1\omega^\alpha f \sin(\frac{\pi}{2}\alpha)}{1 + 2a_1\omega_f^\alpha \cos(\frac{\pi}{2}\alpha) + a_1^2\omega_f^{2\alpha}}.$$

The material parameters were then identified from the experimental data by using the identification procedure based on the above equations, and the predicted responses were compared with the predictions from one-term fractional derivative model and the experimental data. Again, the material parameters were estimated from the optimization procedures with and without an upper limit on α and the predicted results are similar in both cases as discussed in Section 4.3. The results at 30% compression and -0.2 and -0.25 mg N input levels are shown in Fig. 17. In these cases, although the predictions of amplitude in the low-frequency region are improved slightly, more discrepancies in phase are observed, especially in the high-frequency region. It is noted that the resonance predicted at the -0.25 mg N input level extends beyond the experimental response. However, the response at points where the experimental data are available is well predicted. At other compression and input levels, it was also found that the predictions of the response from the two-term fractional derivative models are very close to those predicted from the one-term fractional derivative models. Thus, in contrast to the hereditary model, the two-term fractional derivative model does not have sufficient or appropriate structure to capture the foam's behavior over a large range of compression and input levels.

5. Summary, conclusions and comments

A hereditary model and a fractional derivative model, both with non-linear elastic elements, were introduced to describe the dynamic behavior of flexible polyurethane foam under compression and dynamic loading. In these models, the non-linear elasticity was incorporated in the form of third- and fifth order polynomial stiffness terms. Viscoelastic properties were modelled either by a hereditary integral with a relaxation kernel consisting of two exponential terms or by a fractional derivative term. A brief introduction to the hereditary and fractional

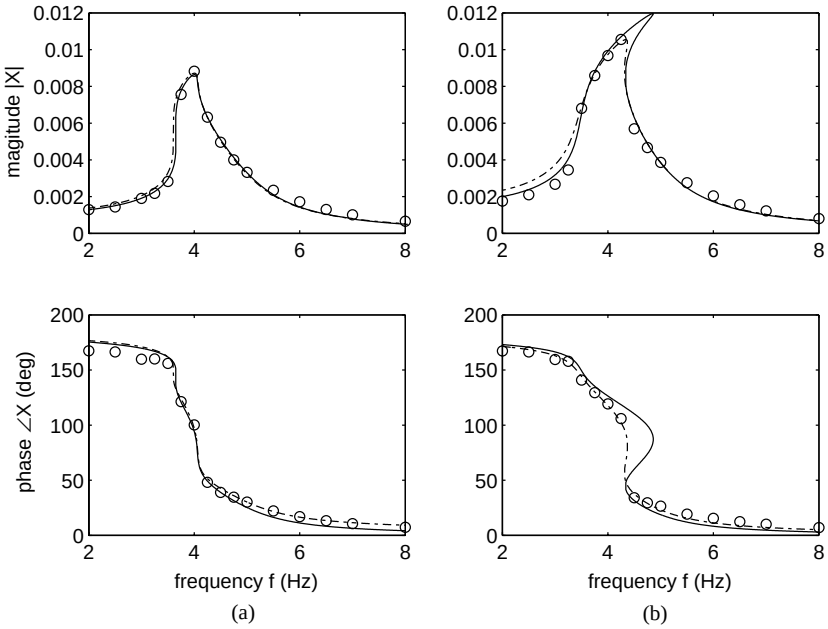

Fig. 17. Measured and predicted responses from the one-term and the two-term fractional derivative model. (a) 30% compression level and $G = -0.2$ mg N. (b) 30% compression level and $G = -0.25$ mg N. o, measured data; -.-, predicted response from the one-term fractional derivative model; —, predicted response from the two-term fractional derivative model.

derivative model characteristics was also given and the associated relaxation behavior in both models was discussed. One-term harmonic balance solutions were derived for both models subjected to harmonic excitation and the resulting equations were used in the system identification procedure. A direct non-linear optimization method based on the sub-space trust region algorithm, and a sub-optimal method which results in a linear optimization after fixing one of the model parameters, were described. The one-term harmonic balance equations were also used to predict the response of the estimated model and to generate simulation data to investigate frequency resolution and noise issues.

Results of simulations showed that the choice of cost function would affect the estimation of the material parameters and a set of equations that weighted the higher amplitude resonance region more strongly yielded more accurate results, probably because this region contained data with the higher signal-to-noise ratio. Therefore, cost functions in this form were used in system identification from the experimental data.

Steady state response data from experiments where the foam was compressed at various levels and excited at four different input amplitudes from 0.1 to 0.25 mg N were used to estimate the model parameters. Both models provided reasonably good predictions of the amplitude and phase of the response at low input levels. The fractional derivative model's performance was poorer at the higher input amplitudes. Simulations also showed that the fractional derivative model utilized did not have enough structure to fit the data generated by the hereditary model at high input and compression levels while the hereditary models fitted the data generated by the fractional

derivative model well. No substantial improvement was observed in the model predictions when an additional fractional derivative term was included. Two relatively simple fractional derivative model forms were investigated. It is possible that a fractional derivative model with a different structure may be more appropriate; this requires further investigation.

The viscous damping term was found to be a redundant parameter in the fractional derivative model since the damping is implicitly represented by the fractional derivative term. It is also not necessary in the hereditary model when fitting to the low compression level experimental data although the presence of the c term yields a better estimation at higher compression levels. This may be explained by the fact that the foam's behavior becomes more complicated at higher compression and input levels and the additional term, even if it is not the most appropriate, helps to fit the data. It is clear that some damping mechanisms other than those presented in the viscoelastic terms, see for example Ref. [7], need to be considered to model the damping properties of the foam material more accurately.

Acknowledgements

The authors acknowledge the support of Dr. Alison Flatau through NSF grant 9900248-CMS, and the technical and financial support of Dr. Bryan McKinney and Mr. Kuntal Thakurta, at ASG, Johnson Controls Inc.

References

[1] A. Cunningham, E. Huygens, J.W. Leenslag, MDI comfort cushioning for automotive applications, Proceedings of the Utech 1994 Conference, The Hague, The Netherlands, March 22–24, 1994, pp. 461–472.
[2] J.W. Leenslag, E. Huygens, A. Tan, Recent advances in the development and characterization of automotive comfort seating foams, Polyurethanes World Congress 1997, Amsterdam, September 29–October 1, 1997, pp. 436–446.
[3] S.W. White, S.K. Kim, A.K. Bajaj, P. Davies, D.K. Showers, P.E. Liedtke, Experimental techniques and identification of nonlinear and viscoelastic properties of flexible polyurethane foam, Nonlinear Dynamics 22 (2000) 281–313.
[4] B. Neal, Difference in dynamic performance of molded polyurethane foam as a function of pad thickness and supported load, Journal of Cellular Plastics 37 (2001) 160–178.
[5] R. Singh, Dynamic Modeling of Polyurethane Foam and Development of System Identification Methodologies, Master's Thesis, Purdue University, School of Mechanical Engineering, West Lafayette, IN, 2000.
[6] R. Singh, P. Davies, A.K. Bajaj, Identification of nonlinear and viscoelastic properties of flexible polyurethane foam, Nonlinear Dynamics, in press.
[7] W.N. Patten, S. Sha, C. Mo, A vibration model of open celled polyurethane foam automotive seat cushions, Journal of Sound and Vibration 217 (1) (1998) 145–161.
[8] S.L. Hager, T.A. Craig, Fatigue testing of high performance flexible polyurethane foam, Journal of Cellular Plastics 28 (1992) 284–301.
[9] K. Vorspohl, J. Mertes, R. Zschiesche, H.D. Lutte, R. Drumm, Time dependence of hardness of cold cure molded flexible foams and its importance for system development, Journal of Cellular Plastics 30 (1994) 361–373.
[10] J.D. Ferry, Viscoelastic Properties of Polymers, Wiley, New York, 1970.
[11] Y.M. Haddad, Viscoelasticity of Engineering Material, Chapman & Hall, London, 1995.
[12] I.M. Ward, Mechanical Properties of Solid Polymers, Wiley, New York, 1983.

[13] A. Muravyov, S.G. Hutton, Closed-form solutions and the eigenvalue problem for vibration of discrete viscoelastic systems, Journal of Applied Mechanics 64 (1997) 684–691.
[14] R. Singh, P. Davies, A.K. Bajaj, Estimation of the dynamical properties of polyurethane foam, through use of Prony series, Journal of Sound and Vibration, in press.
[15] W. Flugge, Viscoelasticity, Blaisdell, Waltham, MA, 1967.
[16] T. Pritz, Analysis of four-parameter fractional derivative model of real solid materials, Journal of Sound and Vibration 95 (1) (1996) 103–115.
[17] J.S. Hwang, S.W. Ku, Analytical modelling of high damping rubber bearings, Journal of Structural Engineering 123 (8) (1997) 1029–1036.
[18] J.S. Hwang, J.C. Wang, Seismic response prediction of HDR bearings using fractional derivative maxwell model, Engineering Structures 20 (9) (1998) 849–856.
[19] R.L. Bagley, P.J. Torvik, A theoretical basis for the application of fractional calculus to viscoelasticity, Journal of Rheology 27 (3) (1983) 201–210.
[20] K.B. Oldham, J. Spanier, An Introduction to Fractional Calculus, Academic Press, New York, 1974.
[21] I. Podlubny, Fractional Differential Equations, Academic Press, New York, 1999.
[22] M. Enelund, G.A. Lesieutre, Time domain modelling of damping using anelastic displacement fields and fractional calculus, International Journal of Solids and Structures 36 (1999) 4447–4472.
[23] P.E. Rouse, A theory of the linear viscoelastic properties of dilute solution of coiling polymers, The Journal of Chemical Physics 21 (7) (1953) 1272–1280.
[24] P.E. Rouse, K. Sittel, Viscoelastic properties of dilute polymer solutions, Journal of Applied Physics 24 (6) (1953) 690–696.
[25] A.H. Nayfeh, D.T. Mook, Nonlinear Oscillations, Wiley, New York, 1979.
[26] M.A. Branch, T.F. Coleman, Y.Y. Li, A subspace, interior, and conjugate gradient method for large-scale bound-constrained minimization problems, SIAM Journal on Scientific Computation 21 (1) (1999) 1–23.
[27] S.W. White, Dynamic Modeling and Measurement of Occupied Car Seats and Seating Foam, Master's Thesis, Purdue University, School of Mechanical Engineering, West Lafayette, 47907, 1998.
[28] S.V. Krysov, V.A. Lazerev, To the Adirovich and Blokhintsev dry friction model: consideration of material viscoelastic properties, Soviet Journal of Friction and Wear 13 (2) (1992) 13–18.
[29] N.C. Hilyard, P. Collier, Structural model for air flow in flexible Pur foams, Cellular Polymer 6 (6) (1987) 9–26.
[30] R.L. Bagley, P.J. Torvik, Fractional calculus-a different approach to the analysis of viscoelastic damped structures, American Institute of Aeronautics and Astronautics Journal 21 (5) (1983) 741–748.